Reconsideration of the Stereoelectronic Effect in Oxyphosphorane Species

Tadafumi Uchimaru,*,† Seiji Tsuzuki,† Joey W. Storer,†,‡ Kazutoshi Tanabe,† and Kazunari Taira*,§

National Institute of Materials and Chemical Research, and National Institute of Bioscience and Human Technology, Agency of Industrial Science and Technology, MITI, Tsukuba Science City 305, Japan, and Department of Chemistry and Biochemistry, University of California, Los Angeles, Los Angeles, California 90024-1569

Received September 7, 1993•

Properties of various oxyphosphoranes such as neutral pentahydroxyphosphorane (doubly protonated **3b**) and dianionic trihydroxyphosphorane (**3b**) and trimethoxyphosphorane (**3a**) were examined by ab initio molecular orbital calculations. The energies of the stationary points were evaluated at the MP2 level of theory with the 6-31+G* basis. The analysis of the oxyphosphorane species indicates that the orientation of the equatorial methoxyl group determines the mode of formation/cleavage of the axial P–O_2/P–O_5 bond. This dependence of the reactivity on the conformation of the equatorial P–O_3 bond is in accord with the prediction that is based on the stereoelectronic effect. However, the present work shows that the long-postulated "n–σ^* orbital interaction" is not predominant in the stereoelectronic control of the oxyphosphorane system.

Recently, we carried out ab initio studies[1,2] on the base-catalyzed methanolysis of ethylene phosphate, as a model for the cleavage of RNA **1**, Chart 1. The potential surfaces for methoxide anion substitution at phosphorus were calculated for a dianionic pentacoordinate trigonal bipyramidal oxyphosphorane species **2a**. The reaction profiles suggested that the endocyclic axial P–O_2 bond is much weaker than the exocyclic P–O_5 bond.[3] The difference between endocyclic P–O_2 and exocyclic P–O_5 bonds may arise from either ring strain[4] or stereoelectronic effects, although the possibility of the predominance of the stereoelectonic effects over ring strain was suggested previously.[5]

Chart 1

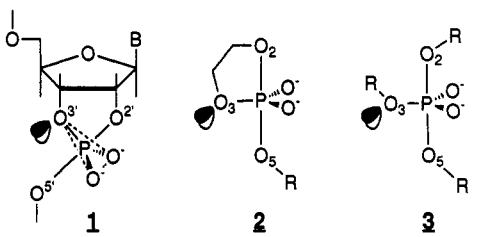

1 **2** **3**

a: R = Me
b: R = H

To eliminate the influence of ring strain, we carried out ab initio investigations on acylic oxyphosphoranes **3a**[6] and **3b**.[7] The 3-21G* reaction profiles indicated that the rotation of the equatorial P–O_3 bond is strongly coupled with phosphorus inversion (inline mechanism). This rotation is consistent with the antiperiplanar lone-pair alignment expected in a stereoelectronically controlled assistance.[6,7] However, our previous calculations were limited to the oxyphosphoranes **3a** and **3b**, with both axial substituents *trans* to the equatorial P–O_3 bond [the (*t*, *t*) conformer]. To examine the generality of the previous results, we have extended our ab initio calculations in the present work to include conformations other than the (*t*, *t*) conformer of oxyphosphorane **3a** and to include a higher level of theory (3-21+G*[8] and 6-31+G*).

The stereoelectronic effect is normally attributed to hyperconjugative orbital interactions.[9] It was pointed out that a stereoelectronic effect in the pentacoordinate oxyphosphorane system would originate from the orbital interactions between the lone-pair orbitals (n) on the equatorial ester oxygen and the antibonding σ orbitals

† National Institute of Materials and Chemical Research.

‡ J.W.S. conducted a portion of this work as a participant in the Summer Institute in Japan for U.S. Graduate Students in Science and Engineering, supported by the National Science Foundation and the Science and Technology Agency of Japan.

§ National Institute of Bioscience and Human Technology.

• Abstract published in *Advance ACS Abstracts,* March 1, 1994.

(1) (a) Taira, K.; Uebayasi, M.; Maeda, H.; Furukawa, K. *Protein Eng.* **1990**, *3*, 691–701. (b) Taira, K.; Uchimaru, T.; Storer, J. W.; Yliniemela, A.; Uebayasi, M.; Tanabe, K. *J. Org. Chem.* **1993**, *58*, 3009–3017.

(2) Storer, J. W.; Uchimaru, T.; Tanabe, K.; Uebayasi, M.; Nishikawa, S.; Taira, K. *J. Am. Chem. Soc.* **1991**, *113*, 5216–5219.

(3) Our calculations on **2a** indicated that the exocyclic P–O_5 transition state is appreciably higher in energy than the endocyclic P–O_2 transition state. Lim and Karplus, in their work on the base-catalyzed hydrolysis of ethylene phosphate (Lim, C.; Karplus, M. *J Am. Chem. Soc.* **1990**, *112*, 5872–5873), indicated that, in contrast to our system, the dianionic pentacoordinate intermediate **2b** does not exist on the potential surface. Considering the unsymmetrical character in the energy profile, we can reasonably interpret nonexistence of the intermediate **2b** as follows. The intrinsically lower transition state for endocyclic P–O_2 bond breaking may conceivably be abolished, leaving only the higher exocyclic P–O_5 transition state, and thus, there is no intermediate on the potential surface.[6]

(4) (a) Cox, J. R., Jr.; Wall, R. E.; Westheimer, F. H. *Chem. Ind. (London)* **1959**, 929–929. (b) Haake, P. C.; Westheimer, F. H. *J. Am. Chem. Soc.* **1961**, *83*, 1102–1109. (c) Usher, D. A.; Dennis, E. A.; Westheimer, F. H. *J. Am. Chem. Soc.* **1965**, *87*, 2320–2321.

(5) (a) Gorenstein, D. G.; Findlay, J. B.; Luxon, B. A.; Kar, D. *J. Am. Chem. Soc.* **1977**, *99*, 3473–3479. (b) Gorenstein, D. G.; Luxon, B. A.; Findlay, J. B.; Momii, R. *J. Am. Chem. Soc.* **1977**, *99*, 4170–4172. (c) Gorenstein, D. G.; Luxon, B. A.; Findlay, J. B. *J. Am. Chem. Soc.* **1977**, *99*, 8048–8049. (d) Gorenstein, D. G.; Luxon, B. A.; Findlay, J. B. *J. Am. Chem. Soc.* **1979**, *101*, 5869–5875. (e) Gorenstein, D. G.; Luxon, B. A.; Goldfield, E. M. *J. Am. Chem. Soc.* **1980**, *102*, 1757–1759. (f) Taira, K.; Gorenstein, D. G. *J. Am. Chem. Soc.* **1984**, *106*, 1521–1523. (g) Taira, K.; Fanni, T.; Gorenstein, D. G. *J. Org. Chem.* **1984**, *49*, 4531–4536. (h) Taira, K.; Gorenstein, D. G. *J. Am. Chem. Soc.* **1984**, *106*, 7825–7831.

(6) Uchimaru, T.; Tanabe, K.; Nishikawa, S.; Taira, K. *J. Am. Chem. Soc.* **1991**, *113*, 4351–4353.

(7) Taira, K.; Uchimaru, T.; Tanabe, K.; Uebayasi, M.; Nishikawa, S. *Nucleic Acids Res.* **1991**, *19*, 2747–2753.

(8) Frisch, M. J.; Pople, J. A.; Binkley, J. S. *J. Chem. Phys.* **1984**, *80*, 3265–3269. The exponents of diffuse functions are given in footnote 13 of this reference.

(9) (a) Lehn, J.-M.; Wipff, G. *J. Am. Chem. Soc.* **1974**, *96*, 4048–4050. (b) Lehn, J.-M.; Wipff, G. *J. Am. Chem. Soc.* **1976**, *98*, 7498–7505. (c) Lehn, J.-M.; Wipff, G. *Helv. Chim. Acta* **1978**, *61*, 1274–1286.

0022-3263/94/1959-1835$04.50/0

(σ^*) of the axial P–O bonds (n_{O3}–$\sigma^*_{PO(ax)}$ interaction).[5] Moreover, it has been believed that the stereoelectronic effect would be larger in the axial P–O bond-forming/breaking transition state than in the metastable pentacoordinate intermediate, with production of a kinetic stereoelectronic effect.[5,9,10] Optimal n–σ^* orbital overlap is found in the antiperiplanar alignment, and a larger n–σ^* interaction could occur in the transition state as compared with that in the metastable state. Because **2** is cyclic, the antiperiplanar lone pairs on O_3 are available only to the endocyclic P–O_2 bond and not to the exocyclic P–O_5 bond. Both the n–σ^* interaction and the relief of ring strain favor cleavage of the endocyclic P–O_2 bond over that of the exocyclic P–O_5 bond.

Does the stereoelectronic control in the oxyphosphorane system really originate from the n_{O3}–$\sigma^*_{PO(ax)}$ orbital interaction? To make this point clear, we have examined the properties of the oxyphosphoranes **3a** and **3b**. Hereafter, we use the term "stereoelectronic" merely as a way of indicating that energetics are dependent on conformation, regardless of the origin of this dependence. Herein we discuss the nature of stereoelectronic control in these pentacoordinate oxyphosphorane systems and demonstrate, for the first time, that the long-postulated "n–σ^* orbital mixing" is not the real cause of the stereoelectronic effects.

Computational Details

It has been confirmed that Hartree–Fock (HF) ab initio calculations reproduce the observed anomeric or stereoelectronic effects in pyranoses and heteroatom-substituted aliphatic compounds.[11,12] Recently, natural bond orbital (NBO) analysis[13] of HF wave functions has been applied to a wide variety of chemical systems and has been shown to provide a clear interpretation of hyperconjugative orbital interaction.[12] In a study on negatively charged molecules that contain hypervalent phosphorus, Streitwieser suggested that d-functions, in particular on phosphorus, are necessary for sufficient polarization stabilization of the anionic charge.[14] Although Karplus and Lim reported that the 3-21G* and the 3-21+G* basis sets provide essentially the same reaction profiles for cyclic oxyphosphorane **2b**,[3] it is also widely accepted that incorporation of diffuse functions must be important for the representation of anionic species such as our model compounds **2** and **3**.[15]

Calculations were carried out with GAUSSIAN 86,[16] GAUSSIAN 88,[17] or GAUSSIAN 90[18] on the following computers: FACOM 780/MSP, IBM 3090/MVS, or CRAY X-MP/216. We have optimized structures of **3a** at both 3-21G* and 3-21+G*[8] levels. Stationary points were fully optimized at the HF level by using the analytical gradient technique,[19] and then vibrational frequencies were calculated by a normal coordinate analysis of force constants, which were determined analytically. Energy profile was explored by using the angle between the equatorial P–O_3 bond and the plane that contains two phosphoryl oxygen atoms and the phosphorus atom as the reaction coordinate. Points comprising the reaction profile in Figure 1 were obtained through geometry optimizations at each value of the reaction coordinate without additional constraints. HF and MP2 energy evaluations were carried out at the 6-31+G* level on the 3-21+G* stationary point geometries. We carried out NBO and Mulliken population analyses for **3a** and **3b** at the 6-31+G* level.[20] Calculations for neutral pentahydroxyphosphorane (doubly protonated **3b**) were carried out at the same level.

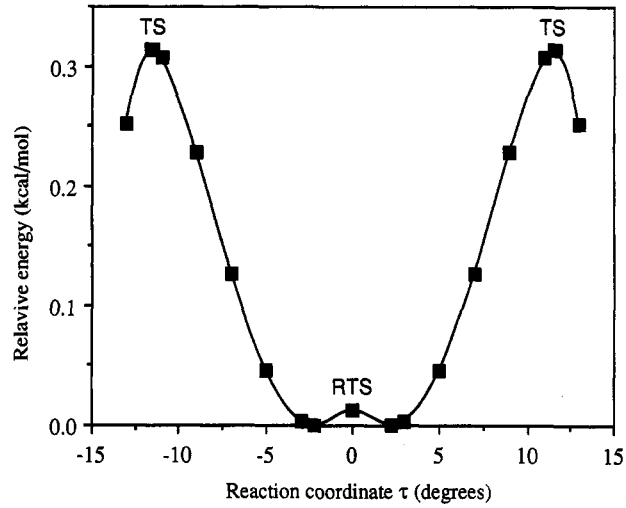

Figure 1. 3-21+G* energy profile for the methoxide attack and displacement step *via* the (*g*, *-g*) conformer of dianionic trimethoxyphosphorane **3a**. The angle (τ) between the equatorial P–O_3 bond and the plane that contains two phosphoryl oxygen atoms and the phosphorus atom is used as the reaction coordinate. The positive and negative values of τ represent P–O_2 and P–O_5 bond forming/breaking, respectively. The vertical axis shows the energies relative to the pentacoordinate intermediate. Because of the structural symmetry, the attack and displacement processes are identical. The reaction profiles were explored starting from the rotational transition states (RTS; $\tau = 0°$), which possess C_s symmetry with respect to the equatorial plane. The geometry optimizations were carried out at each value of the reaction coordinate without additional constraints. The energy profiles for the (*t*, *t*) conformer were shown in Figures 2 and 3 in our previous paper.[6]

Results

To the best of our knowledge, the existence of a dianionic pentacoordinate oxyphosphorane cannot be evidenced in

(10) Kirby, A. J. *The Anomeric Effect and Related Stereoelectronic Effects at Oxygen*; Springer-Verlag: Berlin, 1983.
(11) (a) Aped, P.; Schleifer, L.; Fuchs, B.; Wolfe, S. *J. Comput. Chem.* **1989**, *10*, 265–283. (b) Pichon-Pesme, V.; Hansen, N. K. *THEOCHEM* **1989**, *183*, 151–160. (c) Wiberg, K. B.; Murcko, M. A. *J. Am. Chem. Soc.*, **1989**, *111*, 4821–4828. (d) Leroy, G.; Wilante, C. *THEOCHEM* **1991**, *234*, 303–328. (e) Kysel, O.; Mach, P. *THEOCHEM* **1991**, *227*, 285–293. (f) Meyer, M. *THEOCHEM* **1992**, *257*, 157–166. (g) Cramer, C. J. *J. Org. Chem.* **1992**, *57*, 7034–7043. (h) Wiberg, K. B.; Rablen, P. R. *J. Am. Chem. Soc.* **1993**, *115*, 614–625.
(12) (a) Reed, A. E.; Schleyer, P. v. R. *Inorg. Chem.* **1988**, *27*, 3969–3987. (b) Salzner, U.; Schleyer, P. v. R. *J. Am. Chem. Soc.* **1993**, *115*, 10231–10236.
(13) (a) Foster, J. P.; Weinhold, F. *J. Am. Chem. Soc.* **1980**, *102*, 7211–7218. (b) Reed, A. E.; Weinhold, F. *J. Chem. Phys.* **1983**, *78*, 4066–4073. (c) Reed, A. E., Weinstock, R. B.; Weinhold, F. *J. Chem. Phys.* **1985**, *83*, 735–746. (d) Reed, A. E.; Weinhold, F. *J. Am. Chem. Soc.* **1986**, *108*, 3586–3593. (e) Carpenter, J. E.; Weinhold, F. *THEOCHEM.* **1988**, *169*, 41–62. (f) Reed, A. E., Curtiss, L. A. Weinhold, F. *Chem. Rev.* **1988**, *88*, 899–926.
(14) Streitwieser, A., Jr.; Rajca, A.; McDowell, R. S.; Glaser, R. *J. Am. Chem. Soc.* **1987**, *109*, 4184–4188.
(15) (a) Clark, T.; Chandrashekhar, J.; Spitznagel, G. W.; Schleyer, P. v. R. *J. Comput. Chem.* **1983**, *4*, 294–301. (b) Spitznagel, G. W.; Clark, T.; Schleyer, P. v. R.; Hehre, W. J. *J. Comput. Chem.* **1987**, *8*, 1109–1116.
(16) Frish, M. J.; Binkley, J. S.; Schlegel, H. B.; Raghavachari, K.; Melius, C. F.; Martin, R. L.; Stewart, J. J. P.; Bobrowciz, F. W.; Rohlfing, C. M.; Kahn, L. R.; Defrees, D. J.; Seeger, R.; Whiteside, R. A.; Fox, D. J.; Fleuder, E. M.; Pople, J. A. Carnegie-Mellon Quantum Chemistry Publishing Unit, Pittsburgh PA, 1984.
(17) Frish, M. J.; Head-Gordon, M.; Schlegel, H. B.; Raghavachari, K.; Binkley, J. S.; Gonzalez, C.; Defrees, D. J.; Fox, D. J.; Whiteside, R. A.; Seeger, R.; Melius, C. F.; Baker, J.; Martin, R.; Kahn, L. R.; Stewart, J. J. P.; Fluder, E. M.; Topiol, S.; Pople, J. A. Gaussian Inc., Pittsburgh, PA, 1988.
(18) Frish, M. J.; Head-Gordon, M.; Trucks, G. W.; Foresman, J. B.; Schlegel, H. B.; Raghavachari, K.; Robb, M. A.; Binkley, J. S.; Gonzalez, C.; Defrees, D. J.; Fox, D. J.; Whiteside, R. A.; Seeger, R.; Melius, C. F.; Baker J.; Martin, R. L.; Kahn, L. R.; Stewart, J. J. P.; Topiol, S.; Pople, J. A. Gaussian Inc., Pittsburgh, PA, 1990.
(19) Schlegel, H. B. *J. Comput. Chem.* **1982**, *3*, 214–218.
(20) NBO analysis for **3a** was carried out using SPARTAN: Carpenter, J. E.; Hehre, W. J.; Kahn, S. D. **1990**, SPARTAN version 1.0 Wavefunction Inc. 18401 Von Karman, #370 Irvine, CA 92715.

Table 1. Energetics of the Axial P–O_2 Bond-Forming/-Breaking Reaction Path[a]

stationary point[b]	RHF/3-21G*// RHF/3-21G*				RHF/3-21+G*// RHF/3-21G*				RHF/6-31+G*// RHF/3-21+G*		MP2/6-31+G*// RHF/3-21+G*	
					(*t*,*t*) conformer							
intermediate	−829.450 12	(0.00)	[89.8]		−829.625 19		[88.8]		−833.786 19		−835.261 78	
RTS	−829.447 30	(1.77)	[89.4]	*86.6i*								
TS	−829.447 97	(1.35)	[88.9]	*152.8i*								
					(*g*,−*g*) conformer							
intermediate	−829.448 91	(0.00)	[89.4]		−829.623 43	(0.00)	[88.6]		−833.786 09	(0.00)	−835.264 03	(0.00)
RTS	−829.447 84	(0.67)	[89.5]	*92.0i*	−829.623 41	(0.01)	[88.6]	*29.0i*	−833.786 05	(0.03)	−835.263 91	(0.07)
TS	−829.448 90	(0.01)	[89.3]	*60.0i*	−829.622 93	(0.31)	[88.1]	*162.1i*	−833.787 07	(−0.61)	−835.263 71	(0.20)
					(*t*,*g*) conformer							
intermediate	−829.450 16		[89.8]		−829.625 41		[88.7]		−833.785 46		−835.261 71	

[a] Total energies in au. Relative energies and zero point energies in kcal mol^{-1} are given in parentheses and square brackets, respectively. Imaginary frequencies (cm^{-1}) are given in italics. The calculated frequencies were not scaled. [b] Intermediate, pentacoordinate intermediate; RTS, rotational transition time; TS, transition state for forming/breaking of the axial P–O_2 bond. The components of the eigenvectors that correspond to the imaginary frequencies, computed for the transition states, indicate axial P–O_2/P–O_5 bond formation (or cleavage) and equatorial P–O_3 bond rotation.

Table 2. 3-21G* Geometrical Parameters for Stationary Points of Trimethoxyphosphorane 3a[a]

stationary point[b]	P–O_2	P–O_3	P–O_5	P–O_{eq1}[c]	P–O_{eq2}[c]	O_2–P–O_5	O_3–P–O_5	P–O_3–C	O_2–P–O_3–C	C–O_2–P–O_3	C–O_5–P–O_3
						(*t*,*t*) conformer					
intermediate	1.895	1.670	1.803	1.506	1.503	81.8	82.7	118.7	−50.1	175.7	178.5
RTS	1.848	1.675	1.848	1.507	1.499	81.9	81.9	113.9	−88.8	174.9	−174.9
TS	2.173	1.643	1.755	1.493	1.494	79.1	86.0	120.0	−48.4	−153.7	177.9
						(*g*,−*g*) conformer					
intermediate	1.976	1.677	1.794	1.490	1.500	82.9	86.2	116.7	61.8	74.3	−67.4
RTS	1.851	1.693	1.851	1.494	1.501	84.0	84.0	113.5	88.1	69.2	−69.2
TS	2.004	1.674	1.787	1.489	1.499	82.7	86.6	117.0	60.8	75.0	−67.4
						(*t*,*g*) conformer					
intermediate	1.911	1.678	1.799	1.500	1.503	81.6	85.0	119.5	48.3	−178.0	−70.1

[a] The geometrical parameters are given in Å (bond lengths) and in degrees (bond angles and torsional angles). [b] See Table 1. [c] P–O_{eq1} and P–O_{eq2} are the equatorial phosphoryl P–O bonds that are on the same side as and on the opposite side from the methyl group on the equatorial oxygen O_3, respectively.

Table 3. 3-21+G* Geometrical Parameters for Stationary Points of Trimethoxyphosphorane 3a[a]

stationary point[b]	P–O_2	P–O_3	P–O_5	P–O_{eq1}[c]	P–O_{eq2}[c]	O_2–P–O_3	O_3–P–O_5	P–O_3–C	O_2–P–O_3–C	C–O_2–P–O_3	C–O_5–P–O_3
						(*t*,*t*) conformer					
intermediate	1.918	1.663	1.804	1.530	1.527	82.2	83.4	123.8	−45.6	−177.9	174.9
						(*g*,−*g*) conformer					
intermediate	1.887	1.690	1.837	1.515	1.523	84.6	85.9	118.4	77.6	72.0	−69.9
RTS	1.860	1.691	1.860	1.516	1.523	85.2	85.2	118.1	88.4	70.8	−70.8
TS	2.083	1.671	1.777	1.508	1.516	82.2	88.4	120.3	65.4	74.8	−69.2
						(*t*,*g*) conformer					
intermediate	1.955	1.676	1.785	1.520	1.526	81.9	85.7	126.4	36.1	177.9	−68.4

[a] The geometrical parameters are given in Å (bond lengths) and in degrees (bond angles and torsional angles). [b] See Table 1. [c] P–O_{eq1} and P–O_{eq2} are the equatorial phosphoryl P–O bonds that are on the same side as and on the opposite side from the methyl group on the equatorial oxygen O_3, respectively.

the gas phase. However, it has been experimentally demonstrated that a dianionic oxyphosphorane does exist in the solution phase.[21,22] This is also supported by our previous ab initio investigations.[1b,23] We thus examined the potential surface of dianionic oxyphosphorane **3a**, and NBO analyses were carried out on **3a** and also on both neutral and dianionic oxyphosphorane **3b**.

Figure 1 shows the 3-21+G* energy profile for the methoxide attack and displacement step *via* dianionic trimethoxyphosphorane **3a** with *+gauche −gauche* axial P–O_2/P–O_5 bonds [(*g*, −*g*) conformer]. Similar to the (*t*, *t*) conformer of **3a**,[6] three stationary points, (i) the pentacooedinate intermediate, (ii) the transition state for the rotation of equatorial P–O_3 bond (RTS), and (iii) the axial P–O_2/P–O_5 bond-forming or -breaking transition state (TS), were found for the (*g*, −*g*) conformer of **3a**. The energies and geometrical parameters of the fully optimized stationary point structures, including the pentacoordinate intermediates with *trans trans* [the (*t*, *t*) conformer][6] and *trans gauche* [the (*t*,*g*) conformer] P–O_2/P–O_5 axial bonds, are given in Tables 1–3. The 3-21+G*-optimized structures of the pentacoordinate intermediates are shown in Figure 2. Table 4 shows the results of the NBO analyses along the 3-21+G* reaction coordinate for the (*g*, −*g*) oxyphosphorane **3a**. The structures of the partially optimized dianionic and neutral oxyphosphorane **3b**, as well as their energies and geometrical parameters, are given in Figures 3 and 4, respectively.[24]

(21) (a) Kluger, R.; Westheimer, F. H. *J. Am. Chem. Soc.* **1969**, *91*, 4143–4150. (b) Kluger, R.; Covitz, F.; Dennis, E.; Williams, L. D.; Westheimer, F. H. *J. Am. Chem. Soc.* **1969**, *91*, 6066–6072. (c) Kluger, R.; Taylor, S. D. *J. Am. Chem. Soc.* **1991**, *113*, 5714–5719.

(22) Gorenstein, D. G.; Chang, A.; Yang, J.-C. *Tetrahedron* **1987**, *43*, 469–478.

(23) Yliniemela, A.; Uchimaru, T.; Tanabe, K.; Taira, K. *J. Am. Chem. Soc.* **1993**, *115*, 3032–3033.

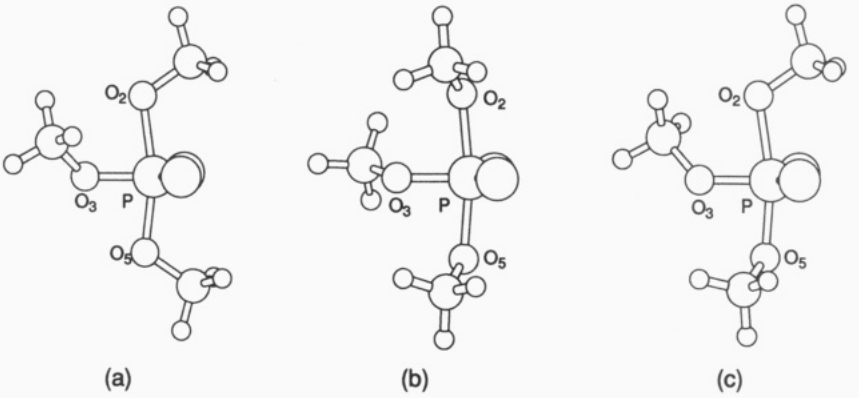

Figure 2. Side views of 3-21+G*-optimized geometries of oxyphosphorane **3a**: (a) (*t*, *t*) pentacoordinate intermediate, (b) (*g*, -*g*) pentacoordinate intermediate, (c) (*t*, *g*) pentacoordinate intermediate.

Table 4. NBO Occupancies for the (*g*,-*g*) Oxyphosphoranes 3a along the Reaction Coordinate[a]

	reaction coordinate[b]						
orbital[d]	0° RTS	2.2° intermediate	5°	7°	9°	11° [c]	11.6° [c] TS
O_3 σ-type lp	1.965	1.966	1.966	1.966	1.966	1.966	1.966
O_3 π-type lp	1.953	1.952	1.952	1.951	1.951	1.950	1.950
P–O_2 BD	1.932	1.937	1.932	1.931	1.931		
P–O_2 BD*	0.150	0.155	0.162	0.168	0.175		
P–O_5 BD	1.932	1.932	1.932	1.932	1.933	1.971	1.971
P–O_5 BD*	0.150	0.145	0.141	0.139	0.136	0.208	0.207
P–O_3 BD	1.948	1.949	1.949	1.949	1.949	1.975	1.976
P–O_3 BD*	0.172	0.172	0.171	0.170	0.168	0.196	0.195

[a] The NBO analysis was carried out for the (*g*,–*g*) oxyphosphoranes **3a** along the 3-21+G* reaction profile shown in Figure 1. The occupancies were calculated with the 6-31+G* basis set. [b] The angle between the equatorial P–O_3 bond and the plane containing two phosphoryl oxygen atoms and the phosphorus atom. RTS, rotational transition state; TS, P–O_2 bond-forming/-breaking transition state. [c] The most satisfactory Lewis structure corresponds to a tetravalent phosphorus (phosphate) and methoxide. [d] lp, lone-pair orbital; BD, bonding orbital; BD*, antibonding orbital.

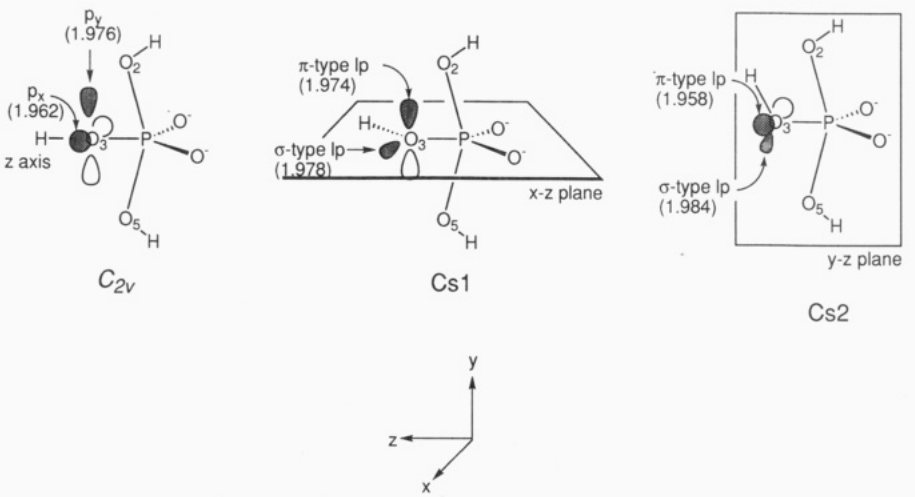

Figure 3. C_{2v}, Cs1, and Cs2 structures of trihydroxyphosphorane **3b**. The lone-pair orbitals on the equatorial oxygen O_3 are drawn schematically. Their NBO occupancies are given in parentheses. The orientations of the *x*, *y*, and *z* axes are shown at the bottom of the figure. The total energies (au) of the C_{2v}, Cs1, and Cs2 structures are –716.669 14, –716.708 66, and –716.772 86, respectively. The geometrical parameters are as follows: the length of the axial P–O_2/P–O_5 bond, 1.865 Å; the length of the equatorial P–O_3 bond, 1.630 Å; the length of the phosphoryl P–O bond, 1.517 Å; the bond angles of O_2–P–O_3 and O_5–P–O_3, 83.2°. The optimized values for the P–O_3–H bond angle are 106.6° and 105.3°, respectively, for the Cs1 and Cs2 structures.

Relative Energies and Geometrical Features of the Stationary Points for Dianionic Oxyphosphorane 3a. Although the relative energies of the stationary points are affected by the computational methods utilized (Table 1),[25] the energy differences among the stationary points are less than the order of k_BT, regardless of the compu-

(24) We must consider the validity of the application of the normal Hartree–Fock calculations to the dianionic species. In general, for small molecules, dianions never exist in the gas phase. The contribution of each electron to electronic properties of the molecule is very large for such a small molecule. However, our systems of **3a** and **3b** are large enough that all the electrons in the occupied orbitals are bound (the HOMO energy levels are negative).

(25) The 3-21G* calculations for the (*t*, *t*) and (*g*, –*g*) conformers both indicate that the rotational transition states (RTS) are slightly higher in energy than the transition states (TS) for axial P–O_2/P–O_5 bond formation (and bond breaking, by the principle of microscopic reversibility). The relative energies of these transition states for the (*g*, –*g*) conformer are reversed upon adding diffuse functions on heavy atoms; the 3-21+G* barrier for rotation of the equatorial P–O_3 bond is found to be lowered as compared to the 3-21G* barrier, whereas the barrier for formation of the axial P–O_2/P–O_5 bond is increased on going from the 3-21G* level to the 3-21+G* level.

Scheme 1

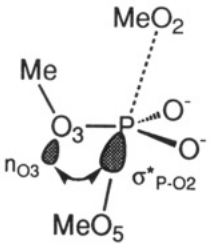

(a)

Favorable for the n_{O3}-$\sigma^*_{P\text{-}O2}$ interaction (bond angle O_2-P-O_3: larger than 90°)

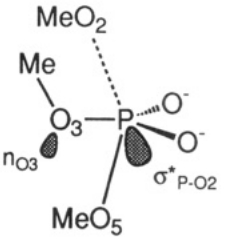

(b)

Unfavorable for the n_{O3}-$\sigma^*_{P\text{-}O2}$ interaction (bond angle O_2-P-O_3: smaller than 90°)

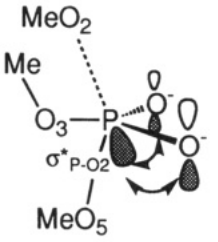

(c)

The interactions between the P-O_2 σ* orbital and the lone-pair orbitals on phosphoryl oxygens

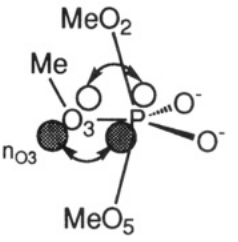

(d)

The interactions between the lone-pair orbitals on O_3 and σ* orbitals of phosphoryl P-O bonds (the n_{O3}-$\sigma^*_{P\text{-}O(eq)}$ orbital interaction)

tational levels.[26] Consequently, a fairly flat potential surface may be expected in the transition-state region for methoxide substitution process. Thus, even if the pentacoordinate intermediate exists along the reaction coordinate, it is kinetically insignificant in the gas phase.[27]

It is noteworthy that the axial bond lengths in **3a** are in accord with the stereoelectronic prediction. In the rotational transition states of the (*t*, *t*) and (*g*, −*g*) conformers, the methyl substituents of the equatorial methoxyl group are located exactly on the equatorial plane. The axial P–O_2 and P–O_5 bonds have the same bond lengths in these rotational transition states, and thus these transition states have C_s symmetry regarding the equatorial plane. Meanwhile, the equatorial P–O_3 bonds are found to be rotated in the pentacoordinate intermediates and in the transition states for the axial P–O_2/P–O_5 bond forming/breaking. One of the axial P–O bonds is thus located on the same side of the methyl substituents of the equatorial methoxyl group and possesses an antiperiplanar lone pair orbital on the equatorial oxygen O_3. The other axial P–O bond occupies the opposite side, and no antiperiplanar lone pair orbital on O_3 is available to this axial P–O bond. In the pentacoordinate intermediate, the former axial P–O bond (P–O_2 in Tables 2 and 3) is always longer than the other axial P–O bond (P–O_5). Correspondingly, the forming or breaking axial P–O bonds (P–O_2 in Tables 2 and 3) in the transition states always occupy the antiperiplanar region of lone pair orbital on the equatorial oxygen O_3. The rotation of the equatorial P–O_3 bond is thus strongly coupled with the reaction coordinate.[6,28,29]

Consequently, at first glance, the axial P–O bond forming and breaking appear to take place with a stereoelectronically controlled assistance in the antiperiplanar lone-pair alignment. However, the bond angles between the axial P–O_2/P–O_5 bond and the equatorial P–O_3 bond do not support the expectation of the n_{O3}–$\sigma^*_{PO(ax)}$ orbital interaction. The axial P–O_2 and P–O_5 bonds are both distorted toward the equatorial P–O_3 bond in the pentacoordinate oxyphosphorane species **3a** and, thus, the bond angles of O_2–P–O_3 and O_5–P–O_3 are smaller than 90°. Since the antibonding orbitals of the axial P–O_2/P–O_5 bonds spread mainly in the outer space of the bonds, the n_{O3}–$\sigma^*_{PO(ax)}$ interaction is diminished by the unfavorable overlap caused by the small O_2–P–O_3 bond angle, Scheme 1b (see the next section). If a hyperconjugative interaction regarding antibonding orbitals of the axial P–O_2/P–O_5 bonds exists, it would be the interaction with lone-pair orbitals of the equatorial phosphoryl oxygens (Scheme 1c) rather than with the lone pair on O_3 (Scheme 1b). A longer P–O_2 bond, as compared to the P–O_5 bond, in the

(26) When zero-point energies are included, the well depths are estimated to be even more shallow. For the (*g*, −*g*) conformer, the pentacoordinate intermediate disappears after zero-point energy correction (see Table 1).

(27) The mechanism of the Diels–Alder reactions was discussed in terms of a "two-stage process": Woodward, R. B.; Katz, T. L. *Tetrahedron* **1959**, *5*, 70–89. Since three stationary points were found along the reaction coordinate for methoxide attack and displacement step via dianionic oxyphosphorane **3a**, the reaction profile may be characterized as a "three-stage process" in a similar fashion, which represents the following: (i) a methoxide anion axially attacks the phosphorus atom with subsequent formation of a pentacoordinate intermediate (the first well); (ii) the equatorial P–O_3 bond rotates, crossing the rotational transition state (RTS; τ = 0°) and producing an enantiomeric intermediate (the second well); and (iii) methoxide leaves *via* the axial P–O bond-breaking transition state (TS) found for i. Probably, however, a kinetically significant intermediate does not exist in the gas phase.

(28) The pentacoordinate intermediate **3a** with the (*t*, *g*) conformation shows the same trends with respect to the axial P–O_2/P–O_5 bond lengths (see Tables 2 and 3) and their overlap populations: the axial P–O_2 bond with an antiperiplanar lone-pair orbital on the equatorial ester oxygen O_3 is longer than the P–O_5 bond without an antiperiplanar lone-pair orbital. The equatorial P–O_3 bond is, thus, expected to rotate along the reaction path for the (*t*, *g*) conformer as well.

(29) Dejaegere, A.; Lim, C.; Karplus, M. *J. Am. Chem. Soc.* **1991**, *113*, 4353–4355.

intermediate is in accord with interpretation based on the n_{O3}–$\sigma^*_{PO(ax)}$ orbital interaction. However, we should also note that the O_2–P–O_3 bond angle is smaller than the O_5–P–O_3 bond angle (Tables 2 and 3). As described in the next section, the n_{O3}–$\sigma^*_{PO(2)}$ interaction generates a larger O_2–P–O_3 bond angle as shown in Scheme 1a. These observations suggest that lengthening of the P–O_2 bond in the intermediate is not a function of n_{O3}–$\sigma^*_{PO(ax)}$ overlap.

Orbital Interaction in Dianionic Oxyphosphorane 3b. Information about the intrinsic orbital interactions of the O_3 lone pairs may be obtained by an examination of the molecular orbitals in the geometry with point group symmetry. In order to simplify the analysis, trihydroxyphosphorane **3b** was optimized at the 6-31+G* level under the C_{2v} symmetry constraint. The equatorial P–O_3–H bond angle was fixed at 180°. Furthermore, starting from the above-mentioned C_{2v} structure, two C_s structures were obtained by optimization of the equatorial P–O_3–H bond angle (Figure 3). The other geometrical parameters were frozen to the C_{2v} optimized values, and the hydrogen atom on O_3 was fixed either on the equatorial (Cs1) or on the axial (Cs2) plane. The 6-31+G* orbitals were examined with respect to C_{2v}, Cs1, and Cs2 structures. NBO analyses on these three structures show that the interactions between the lone-pair orbitals on O_3 and the antibonding orbitals of the equatorial phosphoryl P–O bonds (the n_{O3}–$\sigma^*_{PO(eq)}$ orbital interaction; Scheme 1d) predominate over the n_{O3}–$\sigma^*_{PO(ax)}$ interaction in the oxyphosphorane system.

The z-axis is taken as the axis of the equatorial P–O_3 bond. The negatively charged equatorial phosphoryl oxygens are placed on the x–z plane, and the axial P–O_2 and P–O_5 bonds are placed on the y–z plane (Figure 3). The equatorial oxygen O_3 is sp-hybridized under the C_{2v} symmetry constraint. Although two lone-pair orbitals on the equatorial oxygen O_3 both have pure p character, the p_y orbital on O_3 has a larger population of electron than the p_x orbitals (2.006 *vs* 1.978). Correspondingly, the NBO occupancies are 1.976 and 1.962, respectively, for the O_3 lone-pair orbitals in the axial (y–z) and equatorial (x–z) planes. The second-order perturbation energies corresponding to the n_{O3}–$\sigma^*_{PO(ax)}$ and the n_{O3}–$\sigma^*_{PO(eq)}$ orbital interactions are calculated to be 4.57 and 10.50 kcal mol^{-1}, respectively.

Similar to the optimized structure of **3a**, the axial P–O_2/P–O_5 bonds are distorted toward the equatorial P–O_3 bond in the C_{2v} structure. The bond angles of O_2–P–O_3 and O_5–P–O_3 are 83.2°. This distortion diminishes the n_{O3}–$\sigma^*_{PO(ax)}$ orbital interaction because of unfavorable overlap between O_3 lone-pair and σ^* orbitals of the axial P–O_2/P–O_5 bonds. Upon changing O_2–P–O_3 and O_5–P–O_3 bond angles from 83.2° to 90°, the second-order perturbation energy corresponding to the n_{O3}–$\sigma^*_{PO(ax)}$ interaction increases from 4.57 to 6.13 kcal mol^{-1} (the other geometrical parameters are equal to the values of the C_{2v} structure). Since the orbital energy difference between O_3 lone-pair and antibonding orbitals of the axial P–O_2/P–O_5 bonds increases from 1.18 to 1.21 au, the enhancement of the n_{O3}–$\sigma^*_{PO(eq)}$ orbital interaction should be due to enlargement of the overlap between these orbitals.

The predominance of the n_{O3}–$\sigma^*_{PO(eq)}$ orbital interaction stands out in comparison between the two C_s structures of dianionic **3b**. The equatorial oxygen O_3 has σ- and π-type lone-pair orbitals in the Cs1 and Cs2 structures. The π-type lone-pair orbital in Cs1 and the σ-type lone-pair orbital in Cs2 occupy the axial (y–z) plane, and they may interact with σ^* orbitals of axial P–O_2/P–O_5 bonds. Their NBO occupancies are 1.974 and 1.984, slightly lower than the ideal Lewis value of 2.0. These reduction in occupancies might be related to the n_{O3}–$\sigma^*_{PO(ax)}$ orbital interaction. However, the π- and σ-type lone-pair orbitals both show further reductions in their NBO occupancies when the lone-pair orbitals are located on the equatorial (x–z) plane. Although the difference in the occupancy of the σ-type lone-pair orbital between the Cs1 and Cs2 structures is not very large, the π-type lone-pair electrons are considered to be appreciably delocalized into the antibonding orbitals of phosphoryl P–O bonds (n_{O3}–$\sigma^*_{PO(eq)}$ interaction) in the Cs2 structure. Note that the π-type lone-pair orbitals reduce NBO occupancy from 1.974 in Cs1 to 1.958 in Cs2, and the σ-type lone-pair NBO occupancy varies from 1.984 in the Cs2 structure to 1.978 in the Cs1 structure. The NBO occupancies of antibonding phosphoryl P–O bonds correspond to the change in the π-type lone-pair interaction. Hence, the n_{O3}–$\sigma^*_{PO(eq)}$ orbital interaction may predominate over the n_{O3}–$\sigma^*_{PO(ax)}$ interaction in the oxyphosphorane system.[30]

In the Cs2 structure, the P–O_2 bond is aligned antiperiplanar to the σ-type lone-pair orbital on O_3, whereas there is no such alignment in the case of the P–O_5 bond. The bonding and antibonding P–O_2 NBO occupancies are 1.945 and 0.147, respectively. These occupancies are both larger than the corresponding P–O_5 occupancies (1.940 and 0.140), although C_{2v}-optimized bond lengths (1.865 Å) were used for both the P–O_2 and P–O_5 bonds. Further optimization starting from the Cs2 structure shows that the axial P–O_2/P–O_5 bond lengths are controlled stereoelectronically even under symmetry-restricted conditions. The partial optimization of Cs2, where the planarity of the equatorial plane and C_s symmetry were maintained,[31] caused lengthening of the P–O_2 bond to 1.929 Å and shortening of the P–O_5 bond to 1.832 Å.[32] The differences in NBO occupancies between the antibonding orbitals of P–O_2 and P–O_5 bonds became more marked (0.159 and 0.137). The antibonding occupancy increased by 0.012 for P–O_2 and decreased by 0.003 for P–O_5 upon optimization of the geometry. Meanwhile, the occupancy of the σ-type lone pair of O_3 varies only from 1.984 to 1.985, remaining unaffected even after optimization. Thus, the changes in the antibonding orbital occupancies of P–O_2 and P–O_5 bonds may not result from the n_{O3}–$\sigma^*_{PO(ax)}$ orbital interaction.

NBO Occupancies as a Function of the Reaction Coordinate of 3a. It has been demonstrated that the pentacoordinate oxyphosphorane system is subject to a kinetic stereoelectronic effect.[5] It was presumed that the axial P–O bond-breaking transition state would possess larger n_{O3}–$\sigma^*_{PO(ax)}$ stabilization than the metastable state and that the larger stabilization in the transition state

(30) The same trends are seen in the NBO analysis of the rigid rotamers of **3a** as well. Starting from the 3-21+G*-optimized rotational transition-state (RTS) geometry, the NBO analysis was carried out for the rigid rotamers about the equatorial P–O_3 bond. The NBO occupancy of the σ-type lone-pair orbital on the equatorial oxygen O_3 increases from 1.965 (RTS) to 1.973 upon rotation of the P–O_3 bond by 90°. Conversely, the π-type lone-pair occupancy decreases from 1.953 (RTS) to 1.943. The σ- and π-type lone-pair orbitals both show reductions in occupancy when the lone-pair orbitals are located on the equatorial plane.

(31) Dianionic oxyphosphorane **3b** has no pentacoordinate minimum.[7] Full optimization for **3b** without any structural constraints gave a tetrahedral phosphate.

(32) The total energy (au) of the optimized structure is −716.725 20. The geometrical parameters are as follows: bond lengths, P–O_2, 1.929 Å; P–O_5, 1.832 Å; P–O_3, 1.665 Å; phosphoryl P–O, 1.515 Å; bond angles, O_2–P–O_3, 81.4°; O_5–P–O_3, 81.6°; P–O_3–H, 104.6°.

might be the origin of the kinetic stereoelectronic effect in the oxyphosphorane system.[5d,h] Although our previous calculations on the oxyphosphorane system surely support the existence of a kinetic stereoelectronic effect,[33] the changes of NBO occupancies along the reaction coordinate indicate that n_{O3}–$\sigma^*_{PO(ax)}$ interaction is not a major factor of the kinetic stereoelectronic effect in the oxyphosphorane system (see below).

We have explored the reaction coordinate connecting the rotational transition state and the transition state for the axial P–O_2 bond breaking (RTS and TS in Figure 1). The NBO analysis on each point along the reaction coordinate identifies the rehybridization of phosphorus during cleavage of the P–O_2 bond (see Table 4). The Lewis structures for the rotational transition state (RTS; $\tau = 0°$) and the intermediate ($\tau = 2.2°$) indicate the presence of pentavalent phosphorus (structures at $\tau = 0$–$9°$ show pentavalent occupancies in Table 4), whereas the most satisfactory Lewis structure for the P–O_2 bond-breaking transition state (TS) corresponds to a tetravalent phosphorus (phosphate monoanion; structures $\tau = 11°$ and 11.6° lack P–O_2 bond occupancies) and methoxide. The pentavalent Lewis structure gradually increases the occupancy of the axial P–O_2 antibonding orbital during passage from the rotational transition state (RTS) toward the P–O_2 bond-breaking transition state (TS). Conversely, the P–O_5 antibonding occupancy is reduced along the reaction coordinate (see Table 4).

The NBO occupancy of 1.953 for the π-type lone-pair orbital at the rotational transition state (RTS) is significantly different from the Lewis value of 2.0. This difference might be related to the n_{O3}–$\sigma^*_{PO(ax)}$ orbital interaction, given that the methyl group on O_3 is located exactly on the equatorial plane in the rotational transition state (RTS) and that the π-type lone-pair orbital on O_3 is oriented in the optimal direction for the n_{O3}–$\sigma^*_{PO(ax)}$ interaction at $\tau = 0°$. The equatorial P–O_3 bond rotates with the lengthening of the axial P–O_2 bond. This P–O_3 bond rotation reduces the orbital overlap between the π-type lone pair on O_3 and the σ^* orbital of the axial P–O_2/P–O_5 bonds, while the σ^* orbitals of the equatorial phosphoryl P–O bonds start to interact with the π-type lone-pair orbital on O_3 upon rotation ($\tau = 0° \rightarrow 90°$). Consequently, the n_{O3}–$\sigma^*_{PO(ax)}$ and n_{O3}–$\sigma^*_{PO(eq)}$ orbital interactions may both be influential for the small change (1.953 → 1.950) in the π-type O_3 lone-pair occupancy along the reaction coordinate, whereas the σ-type lone-pair occupancy is essentially the same across the reaction coordinate (Table 4).

In all cases, however, the NBO occupancies of the lone-pair orbitals on O_3 are much less sensitive to the reaction coordinate than the P–O_2/P–O_5 bond occupancies. In addition, O_3 lone pairs show nearly the same NBO occupancies despite the fact that phosphorus rehybridization occurs on going from $\tau = 9°$ to $\tau^* = 11°$ in terms of the reaction coordinate (see Table 4). Hence, the n_{O3}–$\sigma^*_{PO(ax)}$ orbital interaction is not kinetically significant in oxyphosphorane system **3a**.

The Importance of Electrostatic Effect for the Dianionic Species. We carried out geometry optimization starting from the transition state for the axial P–O_2 bond breaking with further lengthening of the P–O_2 bond. The equatorial P–O_3 bond undergoes continuous rotation during cleavage of the P–O_2 bond, as well as during phosphorus inversion. After the distance between P and O_2 is increased to 10 Å, at that distance no orbital interaction is possible, the preferred conformation of the P–O_3 bond in the resulting DMP is still *trans*.[34] The *trans* conformation of the P–O_3 bond in the resulting DMP is rationalized as a consequence of the electrostatic interaction between the negative charge of the departing methoxide and the dipole of the Me–O_3 bond. Thus, the electrostatic interactions as well must be taken into account in the analysis of the reaction coordinate.

Orbital Interaction in Neutral Oxyphosphorane Species. The above analyses were made on dianionic species which may not exist as intermediates in the gas phase. To examine the generality of the above conclusions, we then extended our NBO analysis to a neutral pentahydroxyphosphorane (doubly protonated neutral **3b**). We carried out symmetrically-restricted geometry optimizations for neutral pentahydroxyphosphorane in a fashion similar to the case of dianionic trihydroxyphosphorane **3b** (see Figure 4).[35]

Overall, the same trend can be seen for the neutral species. Moreover, the n_{O3}–$\sigma^*_{PO(eq)}$ interaction (see Scheme 1d) is further enhanced due to neutralization of the negative charges of the phosphoryl oxygens. For the C_{2v} structure of the neutral **3b**, as compared with the corresponding dianionic **3b**, the NBO occupancy of the O_3 lone pair orbital in the equatorial plane is reduced to the value of 1.910, whereas the occupancy of the axial lone pair remains at the similar value of 1.972 (the corresponding values are 1.962 and 1.976, respectively, for the dianionic **3b**). The second-order perturbation energy of the n_{O3}–$\sigma^*_{PO(eq)}$ orbital interaction is 15.24 kcal mol^{-1}, larger than the value of the n_{O3}–$\sigma^*_{PO(ax)}$ interaction (5.29 kcal mol^{-1}). The distortion of the axial P–O_2/P–O_5 bonds toward the equatorial P–O_3 bond is also seen in the C_{2v} structure of the neutral **3b**. The bond angles of O_2–P–O_3 and O_5–P–O_3 are 87.0°. Similar to the case of the dianionic **3b**, the n_{O3}–$\sigma^*_{PO(ax)}$ orbital interaction is enhanced with larger O_2–P–O_3 and O_5–P–O_3 bond angles because of favorable overlap between O_3 lone-pair and antibonding orbitals of the axial P–O_2/P–O_5 bonds. The second-order perturbation energy of the n_{O3}–$\sigma^*_{PO(ax)}$ interaction increases from 5.29 to 6.22 kcal mol^{-1} upon changing O_2–P–O_3 and O_5–P–O_3 bond angles from 87.0° to 90°.[36]

The NBO analyses for the Cs1 and Cs2 structures indicate that the neutral oxyphosphorane **3b** also reduces the occupancies of the π- and σ-type lone-pair orbitals when the respective lone-pair orbitals are located on the equatorial plane. The π-type lone-pair orbital reduces its

(33) See Figure 3 in our previous paper.[6] The energy profile for the rotation of the equatorial P–O_3 bond for dianionic oxyphosphorane **3a** in the metastable state shows a much shallower well than that in the corresponding rotational profile for the axial P–O_2 bond-breaking transition state.

(34) During the 3-21+G* geometry optimization, the torsional angle about O_2–P–O_3–Me and the length of the P–O_2 bond (in parentheses) varied as follows: 53.6° (2.9 Å); 34.1° (5.0 Å); –9.4° (9.9 Å).

(35) Partial geometry optimization starting from neural Cs2 structure showed that the axial P–O_2 and P–O_5 bond lengths are controlled in a stereoelectronic manner. The planarity of the equatorial plane and C_s symmetry were kept during the optimizations: the two hydrogen atoms on the equatorial oxygens other than O_3 were fixed on the equatorial plane. The axial P–O_2 bond possessing antiperiplanar lone-pair orbital on O_3 was slightly lengthened as compared with the axial P–O_5 bond with no antiperiplanar lone-pair orbital (1.684 vs 1.654 Å). The total energy (au) of the optimized structure is –718.008 76.

(36) The geometrical parameters other than O_2–P–O_3 and O_5–P–O_3 bond angles are equal to the values of the C_{2v} structure. The orbital energy difference between O_3 lone-pair and antibonding orbitals of the axial P–O_2/P–O_5 bonds remains almost unaffected (1.30 vs 1.31 au) upon changing O_2–P–O_3 and O_5–P–O_3 bond angles.

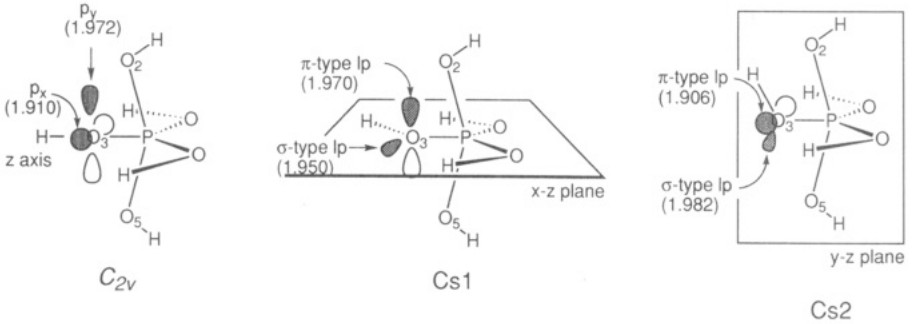

Figure 4. C_{2v}, Cs1, and Cs2 structures of neutral pentahydroxyphosphorane (doubly protonated **3b**). The lone-pair orbitals on the equatorial oxygen O_3 are drawn schematically. Their NBO occupancies are given in the parentheses. These structures were obtained by the geometry optimizations in a fashion similar to the case of dianionic trihydroxyphosphorane **3b** (see Figure 3). The total energies (au) of the C_{2v}, Cs1, and Cs2 structures are −717.967 49, −717.981 50, and −718.006 26, respectively. The geometrical parameters are as follows: the length of the axial P–O_2/P–O_5 bond, 1.668 Å; the length of the equatorial P–O_3 bond, 1.553 Å; the length of the equatorial P–O bond, 1.624 Å; the bond angles O_2–P–O_3 and O_5–P–O_3, 87.0°. The optimized values for the P–O_3–H bond angle are 121.8° and 112.3°, respectively, for the Cs1 and Cs2 structures.

occupancy from the value of 1.970 to 1.906 on going from the axial plane (Cs1) to the equatorial plane (Cs2). Although the change in the occupancy is less remarkable for the σ-type lone pair orbital, the same trend can be seen: the equatorially-oriented σ-type lone pair orbital has the occupancy of 1.950 (Cs1), whereas the occupancy of the axially-oriented σ-type lone pair orbital is 1.982 (Cs2). These results indicate that O_3 lone-pair orbitals interact more strongly with the σ^* orbitals of equatorial phosphoryl bonds (n_{O3}–$\sigma^*_{PO(eq)}$ interaction) than those of the axial P–O_2/P–O_5 bonds (n_{O3}–$\sigma^*_{PO(ax)}$ interaction). The former interactions show the second-order perturbation energies of 15.44 and 15.82 kcal mol^{-1}, respectively, for the Cs1 and Cs2 structures. The second-order energies corresponding to the latter interactions are much smaller. Moreover, the n_{O3}–$\sigma^*_{PO(ax)}$ interaction of the π-type lone-pair orbital on O_3 (Cs1) shows a slightly larger second-order perturbation energy of 5.62 kcal mol^{-1} than that of the σ-type lone pair (Cs2; 3.99 kcal mol^{-1}).

These results confirm that the n_{O3}–$\sigma^*_{PO(eq)}$ interaction is favored over the n_{O3}–$\sigma^*_{PO(ax)}$ interaction not only in dianionic species but also in neutral oxyphosphoranes. Therefore, our conclusion is not dependent on the ionic valence (the amount of the negative charge) of the oxyphosphorane species. Similar trends were also observed for equatorially amino-substituted neutral phosphoranes, such as PH_4NH_2 and PF_4NH_2, where the lone pair on the nitrogen atom interacts more favorably with the σ^* orbitals of the equatorial P–H/P–F bonds than with the axial σ^* orbitals.[37]

Discussion

We have located the stationary points along the reaction coordinates for the base-catalyzed methanolysis of DMP monoanion at the 3-21G* and 3-21+G* levels. The energies of the stationary points were evaluated by HF and MP2 methods at the 6-31+G* level. The calculated potential surfaces show the strong coupling of the rotation of the equatorial P–O_3 bond with the phosphorus inversion. This bond rotation is in accord with the theory of a stereoelectronically controlled assistance.

Gas-phase calculations such as ours have always supported the stereoelectronic control in these systems.[1,3,5-7,9,10] Until now, the stereoelectronic control in the oxyphosphorane system has been interpreted as being a consequence of the hyperconjugative orbital interaction between the lone-pair orbital on the equatorial ester oxygen O_3 and the σ^* orbital of the axial P–O_2/P–O_5 bonds (the n_{O3}–$\sigma^*_{PO(ax)}$ orbital interaction), which would require antiperiplanar lone-pair alignment with the breaking bond.[5] However, we have shown in the present work that it is not sufficent to interpret the stereoelectronic control in the oxyphosphorane system exclusively in terms of the n_{O3}–$\sigma^*_{PO(ax)}$ orbital interaction for the following reasons: (i) The geometrical features of **3a** indicate that the interactions between lone-pair orbitals on phosphoryl oxygens and σ^* orbitals of the axial P–O_2/P–O_5 bonds are more significant than the n_{O3}–$\sigma^*_{PO(ax)}$ orbital interaction. (ii) The lone-pair electrons of the equatorial oxygen O_3 have a tendency to be delocalized into the antibonding orbitals of the phosphoryl P–O bonds (the n_{O3}–$\sigma^*_{PO(eq)}$ orbital interaction). The NBO occupancies and second-order perturbation energies indicate that the n_{O3}–$\sigma^*_{PO(eq)}$ orbital interaction predominates over the n_{O3}–$\sigma^*_{PO(ax)}$ interaction. (iii) The kinetic aspects of the stereoelectronic effect cannot be explained by the n_{O3}–$\sigma^*_{PO(ax)}$ orbital interaction: the expected larger n_{O3}–$\sigma^*_{PO(ax)}$ orbital interaction at the transition states than the metastable state is not recognized by our NBO analysis. These conclusions are derived from the analyses of not only dianionic but also neutral oxyphosphoranes. Thus, the n_{O3}–$\sigma^*_{PO(ax)}$ orbital interaction is not the principle source of stereoelectronic control in the oxyphosphorane system. The rotation of the equatorial P–O_3 bond during the phosphorus inversion may be attributed at least in part to an electrostatic interaction.

The gas-phase reaction profile conflicts with the solution-phase experimental results in several aspects. For instance, the existence of a dianionic oxyphosphorane intermediate in the solution phase has been demonstrated experimentally,[21,22] while the gas-phase potential surface suggests only a kinetically insignificant intermediate. The calculation results of the present work suggest that the electrostatic interactions should be important for the interpretation of the gas-phase reaction coordinate. Since the electrostatic effect is expected to be weakened by solvation, the gas-phase reaction profiles may be modified upon inclusion of solvation. Indeed, our recent molecular

(37) (a) Hoffmann, R.; Howell, J. M.; Muetterties, E. L. *J. Am. Chem. Soc.* **1972**, *94*, 3047–3058. (b) Strich, A.; Veillard, A. *J. Am. Chem. Soc.* **1973**, *95*, 5574–5581. (c) McDowell, R. S.; Streitwieser, A. J., Jr. *J. Am. Chem. Soc.* **1985**, *107*, 5849–5855. (d) Wang, P.; Zhang, Y.; Glaser, R.; Reed, A. E.; Schleyer, P. v. R.; Streitwieser, A. *J. Am. Chem. Soc.* **1991**, *113*, 55–64.

orbital calculations indicate that, once the pentacoordinate species has been solvated, such an intermediate always exists.[1b,23] In particular, our results call attention to the fact that a very important chemical intermediate in phosphorus chemistry, which has to date been supposedly excluded on the basis on gas-phase calculations, is in fact allowed once the solvent is included.

Thus, gas-phase calculations have to be treated with care when they are extrapolated to solution. However, we are not denying these kinds of calculations to analyze reaction mechanisms. In fact, our earlier proposal based on gas-phase calculations[38] is in accord with the recent experimental result[39] indicating that Mg^{2+} ion acts as a Lewis acid to stabilize the leaving oxyanion in *Tetrahymena* ribozyme. According to the results of the very recent studies, all ribozymes appear to be metalloenzymes.[38-41]

(38) (a) Uebayasi, M.; Uchimaru, T.; Tanabe, K.; Nishikawa, S.; Taira, K. *Nucleic Acids Res. Symp. Ser.* **1991**, *25*, 107–108. (b) Uchimaru, T.; Uebayasi, M.; Taira, K. *Chem. Exp.* **1992**, *7*, 501–504. (c) Uchimaru, T.; Uebayasi, M.; Tanabe, K.; Taira, K. *FASEB J.* **1993**, *7*, 137–142.

(39) Piccirilli, J. A.; Vyle, J. S.; Caruthers, M. H.; Cech, T. R. *Nature* **1993**, *361*, 85–88.

(40) Pyle, A. M. *Science* **1993**, *261*, 709–714.

(41) Steitz, T. A.; Steitz, J. A. *Proc. Natl. Acad. Sci. U.S.A.* **1993**, *90*, 6498–6502.